Instrument Science Report WFC3 2018-06

WFC3/IR Blob Monitoring

Ben Sunnquist

June 03, 2018
Last Updated: January 17, 2023

Abstract

Throughout the lifetime of WFC3, a growing number of 'blobs' (small, circular regions with slightly decreased sensitivity) have appeared in WFC3/IR images. In this report, we present the current workflow used for identifying, characterizing and flagging new IR blobs. We also describe the methods currently used to monitor the repeatability of the channel select mechanism (CSM) movements as a way to ensure that the CSM is still operating normally as these new blobs form. A full listing of all known blobs, which incorporates the work from past blob monitoring efforts, is presented in the Appendix as well as all of the IR bad pixel tables generated to include the strongest of these blobs. These tables, along with all of the other relevant figures and tables in this report, will be continuously updated as new blobs form.

1 Introduction

A growing number of small, circular regions with slightly decreased sensitivity have appeared in WFC3/IR images throughout the mission. As described in Pirzkal et al. (2010), these so-called 'IR blobs' appear due to particulates on the channel select mechanism (CSM) - the movable mirror that is used to direct light into either the UVIS or IR channels of the instrument. These particulates are likely cracked epoxy originating from two pins joining the CSM motor shafts to the alignment bellows; therefore, it is critical that blob accumulation is monitored as a growing number of blobs may signify a loosening of these pins, and thus a defective CSM.

In this report, we summarize the results of past blob monitoring efforts (Pirzkal et al., 2010; Pirzkal & Hilbert, 2012; McCullough et al., 2014) and present the current workflow

that is used for identifying and characterizing new IR blobs. We also describe the methods currently used to monitor the CSM repeatability as a way to ensure that the CSM is still operating normally as these new blobs form. The figures and tables contained in this report will be continuously updated as new blobs are discovered.

2 Data

We currently use dark-Earth flats (i.e. observations of the dark side of the Earth) from dedicated CSM/blob monitoring programs to identify new blobs. These images provide a high background level due to the dark-Earth airglow (e.g. from OH molecules) which makes them ideal for detecting new blobs. These observations are obtained using the F153M filter and a 6-read SPARS25 sample sequence with exposure times of 102.9 seconds. The dedicated CSM/blob monitoring programs to date include 13068, 13499, 13588, 14030, 14392, 14549, 14999 and 15592. Within these programs, the dark-Earth observations only have the possibility of being taken after the CSM switches to the IR channel (this helps minimize the total number of CSM moves), so the observing cadence varies; typically 2-3 observations are executed per week, though sometimes the gap between observations can exceed 2 weeks.

Additional dark-Earth flats from programs 11917, 12709, 13099, and 13182 were used in McCullough et al. (2014) to provide a complete census of the existing blobs. However, since these programs weren't specifically designed to monitor the CSM/blobs they sometimes employ different sample sequences, filters and exposure times than those dedicated programs.

The earliest blob monitoring efforts (Pirzkal et al., 2010; Pirzkal & Hilbert, 2012) used deep IR sky flats to detect and characterize blobs. These images were created by combining many deep WFC3/IR observations taken using the broad filters. This strategy was later discarded in favor of the dark-Earth flats as the high background levels in these images allowed us to identify the appearance of fainter blobs over short timescales.

We created the full listing of known blobs in Table 1 by compiling the results of all of the monitoring efforts listed above; therefore, many of the older blobs were detected using different types of observational methods than those consistent methods employed in the dedicated CSM/blob monitoring programs that began in August 2012.

3 Identifying Blobs

To identify blobs, we first perform a custom calibration on the CSM/blob monitoring dark-Earth images. For each of these raw images, we first bias correct them by subtracting the zeroth read from the final read. Next, we divide this bias-corrected final read by the median of a stack of F153M internal flat fields. Finally, we smooth the image by replacing each pixel's value with the median in a 15x15 pixel box centered around that pixel and then subtract 1 to invert the signs - giving the blobs positive values. The resulting image (hereafter referred to as a 'blob image') is one where the blobs strongly stand out from the background (see the top left image in Figure 1 for an example of a blob image).

Every time a new CSM/blob monitoring dark-Earth image comes in, we perform the above calibration to create the current blob image. We also create a median stack of the 30 blob images prior to this current image. To see if any new blobs appeared in the most

recent observation, we create a difference image between the current blob image and this stack. In this difference image, new blobs stand out as positive as they appear in the new observation but not the past observations (Figure 1). In these images, we also circle all of the currently known blobs; this helps to quickly see if a blob showing in the difference image is actually unrecorded, as it takes awhile for new blobs to be incorporated into the stack (i.e. for them to disappear from the difference image). Also, we like to see a potential new blob in multiple consecutive blob images before reporting it to ensure that it is a real blob and not just another source of positive values (unstable pixels, persistence, etc.).

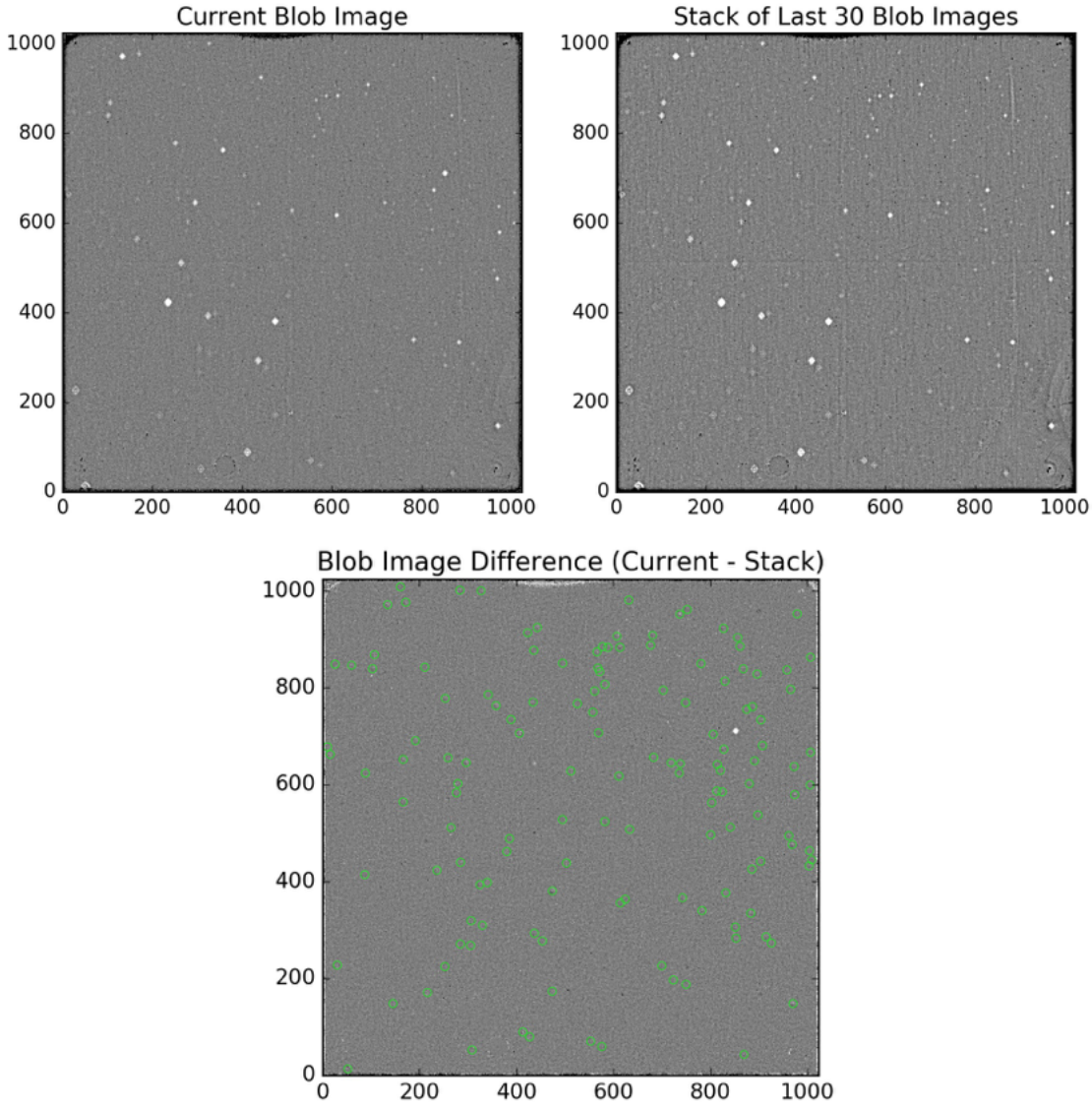

Figure 1: An individual blob image (top left), a stack of the 30 blob images prior to this image (top right), and the difference between these two (bottom). All of the known blobs at the time of this observation are circled in green in the difference image. The two uncircled blobs at (x,y)=(853,711) and (438,643) are new blobs that need to be reported. The other sources of positive flux are likely unstable pixels; these can be distinguished from new blobs by their sharp profiles or by inspecting the original dark-Earth image's data quality array.

4 Characterizing Blobs

When new blobs are discovered, we use the blob images to record their position, radius, flux, appearance date and appearance date uncertainty.

We record the position of a new blob by visually inspecting all of the 1024x1024 blob images where the blob currently appears. The number of images used to determine this position varies, but as previously stated, we like to see the blob in at least a few observations before reporting it as real.

As described in McCullough et al. (2014), the blob radii vary across the detector, with the most in focus blobs in the upper right and the most unfocused in the bottom left. We use the same focus equation to determine blob radii as McCullough et al. (2014):

$$R = \begin{cases} (13 - 0.006L)\sqrt{F/32} & F < 32 \\ (13 - 0.006L) & F > 32 \end{cases} \quad (1)$$

where $L = X\cos 45^\circ + Y \sin 45^\circ$ (X and Y being the blob's position on the detector) and F is the blob flux in units of the normalized blob images. In rare instances, we found that this equation underestimated the blob radii for new blobs that were strong enough to be flagged in the IR bad pixel table; in these scenarios, we increase the calculated radii from Equation 1 to ensure that the entirety of these new blobs are flagged. To determine the blob flux, we again use the results from McCullough et al. (2014); in their report, they run a *DAOfind* algorithm on a stack of ∼100 blob images (i.e. calibrated dark-Earth flats as described in Section 3) to determine each blob's integrated flux. For new blobs, we record an estimate of its flux by visually comparing its flux in the blob images where it currently appears to those along a similar focus that were already calculated in McCullough et al. (2014). This means that the recorded fluxes of newer blobs in Table 1 are less reliable than the older blobs; however, we can't base our flux measurements for new blobs on a large stack of blob images as they have only appeared in a few images at the time of reporting.

We record the appearance date of a new blob as the exposure start time of the last CSM/blob monitoring image that the blob *wasn't* seen in. This ensures that all science exposures that may be affected by this blob have it flagged in their data quality (DQ) arrays; this is the same approach used in McCullough et al. (2014). However, the oldest blobs discovered in Pirzkal & Hilbert (2012) have appearance dates corresponding to the times they first appeared in observations; this is because they recorded the appearance date as the time when the signal in a blob region dipped in a series of deep, time-sorted WFC3/IR observations. Because these observations preceded the first dark-Earth flats, these appearance dates cannot be reconstructed to be consistent with the blobs that followed. We did modify some of these early blobs' appearance dates as a close inspection of early WFC3/IR observations revealed that some had appeared in images earlier than was previously recorded (see Revisions). The first dark-Earth flats revealed a large number of previously undetected blobs; we simply record the appearance dates of these blobs as the time of the first dark-Earth flat.

The accuracy of the blob appearance dates is limited by the cadence of the dark-Earth CSM/blob monitoring images. Because of this, we also record the 'window size' for new blobs. The window size is recorded as the time range when a blob could have appeared, i.e. the time between the last monitoring image the new blob *wasn't* seen in and the first

monitoring image it *was* seen in. We find that the typical window size is ∼1-2 days but can get as high as ∼2 weeks. We were only able to calculate reliable window sizes for blobs discovered after the consistent monitoring effort began in August 2012; the images used to detect blobs prior to this time either lacked a regular cadence or used different targets and observational methods which made the window size calculations highly unreliable.

5 Flagging Blobs

Once the relevant information has been recorded for a new blob, we must determine if the blob is strong enough to flag in an updated IR bad pixel table (BPIXTAB). It is necessary to flag the strongest blobs as they can absorb up to 10-15% of the incoming light at their centers (Pirzkal et al., 2010), which is not necessarily accounted for in the flat-field calibration images. To determine if a new blob is strong enough to flag, we first make a median stack of all of the blob images where the new blob appears. Next, we estimate the background level by calculating the sigma-clipped, full-image median signal. We then replace any values less than -0.2 (e.g. hot pixels, since the blob images have inversed signals) or greater than 0.5 (e.g. dead, unbonded pixels) with this background level before background-subtracting the entire image. Once this is complete, we calculate the sum of pixel values within a circular aperture centered around each blob. Using this information, we can determine if the brightness of a new blob falls within the range of those currently flagged in the IR bad pixel table, and thus, whether it should also be included in an updated version of this table (Figure 2).

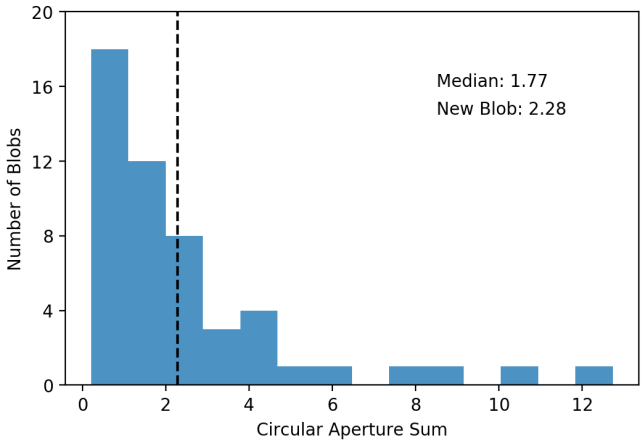

Figure 2: The distribution of the circular aperture sums of blobs flagged in the IR bad pixel table. The value for a new blob is also shown (vertical line), and it's clear that this new blob is strong enough to be included in an updated IR bad pixel table.

When a new blob warrants inclusion in an updated IR bad pixel table, we generate the table (blobs are flagged with a value of 512) with a USEAFTER date set to the time of the last monitoring image the blob wasn't seen in. This way, once the BPIXTAB is delivered and incorporated into the *calwf3* pipeline, all IR observations that may have been affected by this blob will be reprocessed to have it flagged in their DQ arrays. This is the same time-dependent bad pixel table approach described in McCullough et al. (2014). A full listing of

all of the BPIXTABs created due to new blobs is shown in Table 2 in the Appendix.

6 Blob/CSM Trends

The total number of blobs accumulated over time is shown in Figure 3. New blob appearances have mainly occurred in a few distinct surges intermixed with long periods of ∼no new accumulation; the periods with high blob accumulation began shortly after launch, mid-2011 and mid-2017. Though a large number of blobs have been discovered, they cover only a small fraction of the IR detector (Figure 3, top).

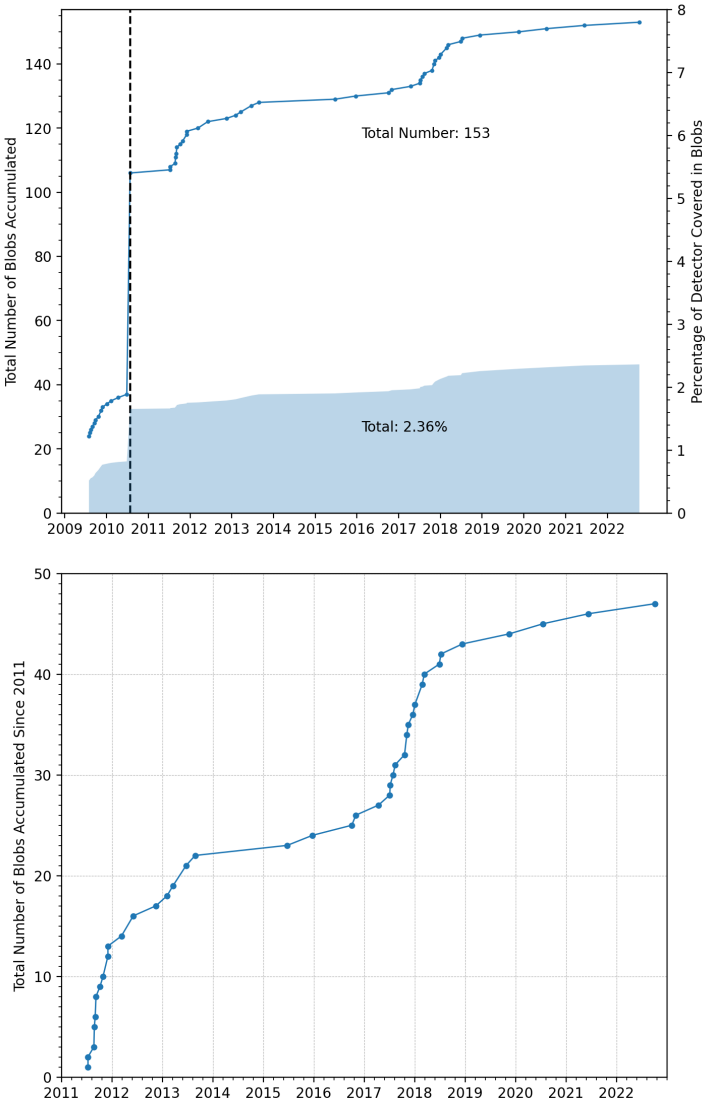

Figure 3: Top: The total number of blobs accumulated over time and the total percentage of the detector covered by these blobs. The black vertical line signifies the switch from using sky flats to dark-Earth flats for blob identification. The first dark-Earth flat revealed a large number of previously undetected blobs - hence the large increase in blob accumulation at this time. Bottom: The total number of blobs accumulated since 2011.

Figure 4 shows all of the currently known blobs - the positions of which are scattered uniformly across the detector. Only the strongest blobs in this image (circled in red) are flagged in the IR bad pixel table. The blob radii scale with the focus from the top right to the bottom left of the detector as determined by Equation 1.

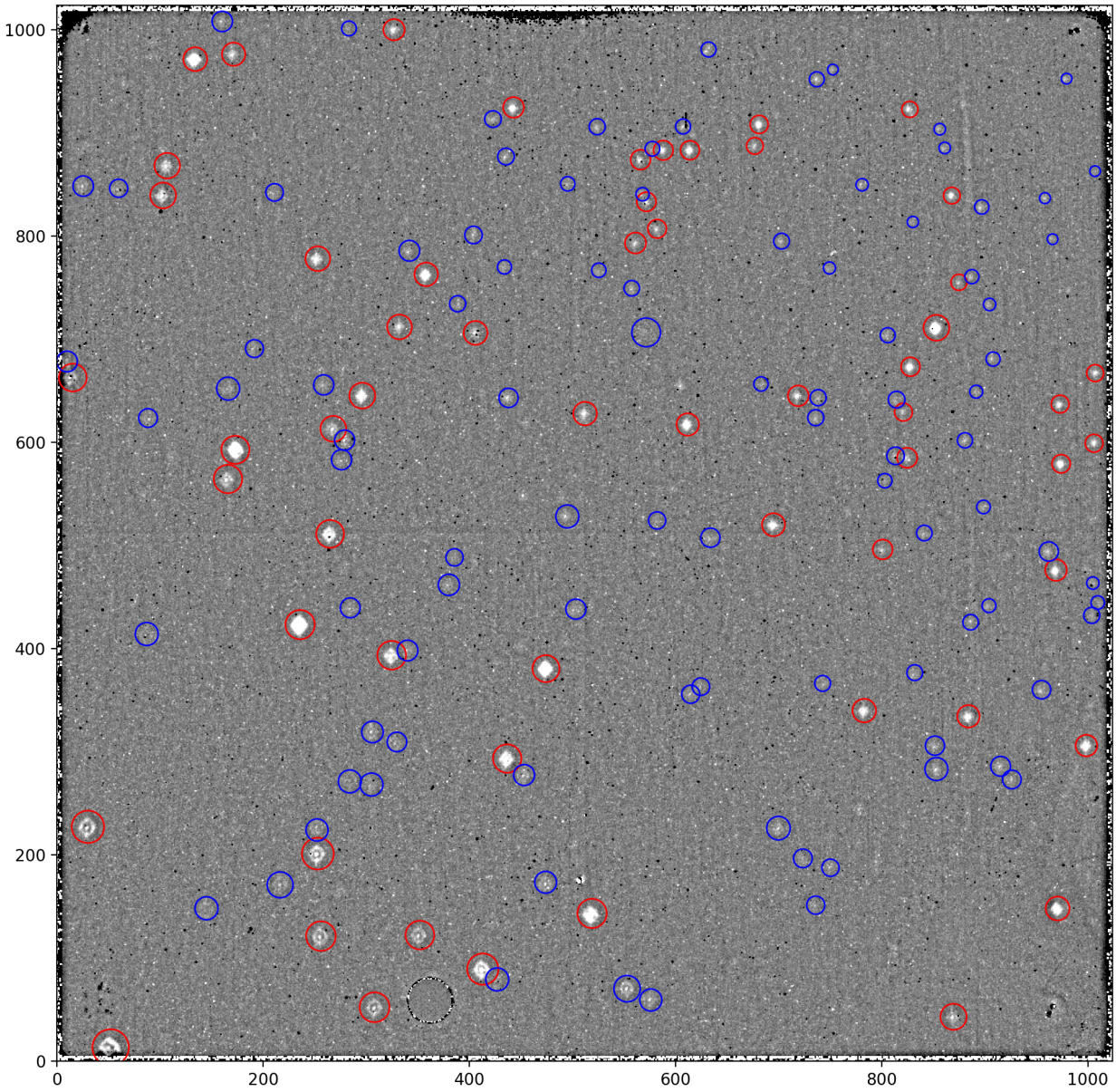

Figure 4: All of the currently known blobs. Blobs that are flagged in the IR bad pixel table (BPIXTAB) are circled in red; all of the other weaker blobs are circled in blue. The blob radii generally increase from the top right to the bottom left of the detector (Equation 1).

Because new blobs may be caused by cracked epoxy holding two pins critical to the integrity of the CSM, we monitor the CSM repeatability (i.e. we monitor that the CSM is returning to same position in IR observations) to ensure that the CSM continues to operate

normally as new blobs form. As new blobs form (i.e. as more epoxy is lost), the pins may become loose, causing the CSM to operate abnormally. By monitoring the CSM repeatability, we may be able to catch this abnormal behavior before the CSM ceases to operate entirely - allowing measures to be put in place to extend the lifetime of WFC3.

To measure the CSM repeatability, we measure the CSM angle of rotation in each of the calibrated dark-Earth flats from the CSM/blob monitoring programs (i.e. the blob images from Section 3). For each blob image, we first cutout a 10x10 pixel box around 31 reference blobs (theses are early blobs that appear in every blob image). For each cutout, we fit a Gaussian to the summed row and column values and record the peak of these fits as the blob center position. We flag any blob where this Gaussian fit fails (e.g. when it is covered in a light trail). At this point, we have the x,y position of the blob centers for each reference blob in every blob image. Next, for each blob image, we use the difference between each calculated blob center and a static reference position to get a measure of the angle of rotation of the CSM. We record the average of all 31 of these measurements in each blob image as the CSM angle of rotation for this image, and record the normalized standard deviation as the error on this measurement. Because we receive a regular cadence of new blob images, we can use this measurement to monitor the CSM repeatability over time (Figure 5; see the supplemental csm_offsets.txt file for an updated list of all of these measurements over time).

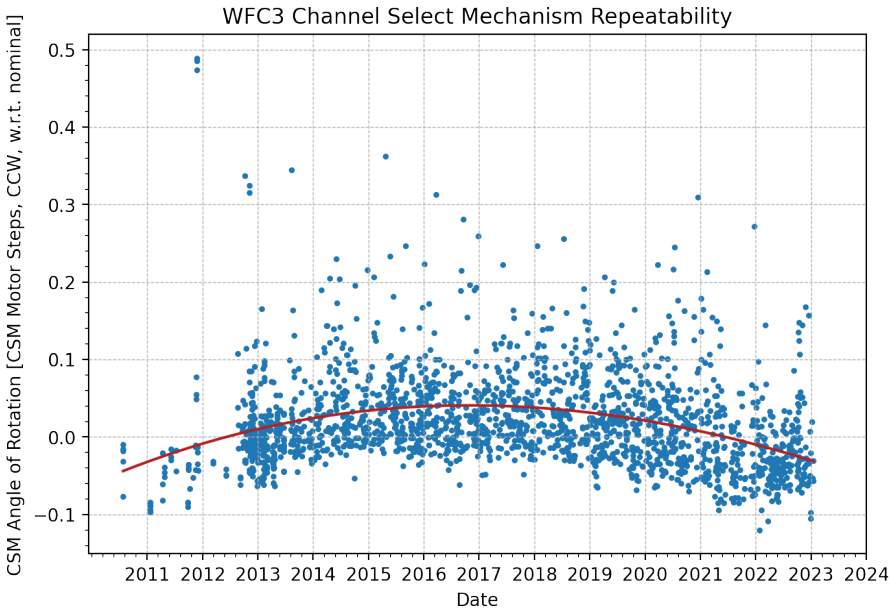

Figure 5: The CSM repeatability over time. The CSM angle of rotation shows no longterm trends as new blobs form. High outliers are likely due to light trails that occasionally streak across the dark-Earth flats, making fitting the blob positions difficult. The lower early values occur when a variety of observational methods (filter, sample sequence, etc.) were used for the dark-Earth flats, rather than the consistent approach employed thereafter. The individual values from this plot, along with the associated errors, can be found in the supplemental csm_offsets.txt file.

In Figure 5, we see that the CSM angle of rotation has remained relatively stable over

time, even during periods of high blob accumulation. The earliest measurements (prior to August 2012) were calculated using dark-Earth flats with a variety of filters, sample sequences and exposure times which may explain their lower values compared to the measurements performed on the consistent dark-Earth flat observations that followed. High outliers are often caused by various IR anomalies (light trails, persistence, etc.) that make their way into the calibrated blob images and make blob fitting difficult.

7 Summary

A growing number of blobs have appeared on the WFC3/IR detector throughout the lifetime of the instrument. Using a regular cadence of calibrated dark-Earth flats, we identify and characterize new blobs as well as flag the strongest in updated IR bad pixel tables. Blob accumulation has mainly been constrained to a few relatively short time periods intermixed with long periods of no new accumulation. We find that the CSM angle of rotation (i.e. its repeatability) has remained relatively constant over time - showing that the CSM continues to operate normally as new blobs form.

References

McCullough, P.R., Mack, J., Dulude, M., and Hilbert, B., 2014. WFC3 ISR 2014-21. **"Infrared Blobs: Time-dependent Flags"**.

Pirzkal, N., Viana, A., and Rajan, A., 2010. WFC3 ISR 2010-06. **"The WFC3 IR "Blobs""**.

Pirzkal, N., and Hilbert, B., 2012. WFC3 ISR 2012-15. **"The WFC3 IR "Blobs" Monitoring"**.

Acknowledgments

We would like to thank Peter McCullough for the development of many of the CSM/blob monitoring methods and analysis algorithms described in this report and Gabriel Brammer for the review of this document.

Appendix

Table 1: All of the known blobs on the WFC3/IR detector (sorted by their appearance dates). The appearance dates for blobs #38 onwards correspond to the last CSM/blob monitoring images that the blobs *weren't* seen in; this ensures that all of the blobs are masked in any science images where they may be present. The appearance dates for blobs #1-37 correspond to the estimated times that they actually appeared in WFC3/IR images; these were found using a different sky flat method as described in Pirzkal & Hilbert, 2012 (note: we have modified some of these earlier appearance dates, see Revisions). The switch to blob finding using dark-Earth flats revealed a large number of previously unknown blobs; the appearance dates for these blobs correspond to the time of the first dark-Earth image (55402.7). The blob windows, which can be thought of as the errors on the appearance dates, represent the time between the last monitoring image a blob wasn't seen in and the first monitoring image it was seen in. Due to inconsistencies in past blob monitoring efforts, reliable windows could only be calculated for blobs since August 2012 (i.e. when the consistent blob monitoring effort began). Blobs that are included in the WFC3/IR BPIXTAB are marked 'Yes' in the final column. A text version of this table is presented in the supplemental blob_summary.txt file.

N	X	Y	Radius	Flux	Appearance (MJD)	Appearance Window (Days)	Flagged
1	30.0	227.0	11.3	29.0	55043.0	-	Yes
2	52.0	13.0	12.7	50.0	55043.0	-	Yes
3	106.9	868.2	8.9	55.3	55043.0	-	Yes
4	160.3	1008.1	7.1	24.9	55043.0	-	No
5	171.3	976.3	8.1	52.9	55043.0	-	Yes
6	306.0	319.0	7.5	16.7	55043.0	-	No
7	308.0	52.0	10.4	26.4	55043.0	-	Yes
8	324.6	393.4	10.0	62.5	55043.0	-	Yes
9	358.1	762.8	8.2	130.3	55043.0	-	Yes
10	406.0	706.0	8.3	37.8	55043.0	-	Yes
11	474.0	173.2	7.6	17.6	55043.0	-	No
12	568.0	840.5	4.6	13.7	55043.0	-	No
13	571.5	706.5	10.0	16.1	55043.0	-	No
14	588.1	883.1	6.8	55.1	55043.0	-	Yes
15	614.0	883.2	6.6	79.6	55043.0	-	Yes
16	699.8	225.7	8.2	26.1	55043.0	-	No
17	719.0	645.0	7.2	55.3	55043.0	-	Yes
18	827.3	922.8	5.6	38.3	55043.0	-	Yes
19	827.9	673.2	6.6	100.3	55043.0	-	Yes
20	868.0	839.2	5.8	60.2	55043.0	-	Yes
21	869.6	42.7	9.1	36.1	55043.0	-	Yes
22	884.1	334.2	7.8	83.4	55043.0	-	Yes
23	973.0	637.0	6.2	51.2	55043.0	-	Yes
24	974.0	579.1	6.4	92.7	55043.0	-	Yes
25	235.8	423.1	10.2	159.7	55050.0	-	Yes
26	611.8	617.2	7.8	112.9	55059.0	-	Yes
27	134.1	971.5	8.3	181.4	55073.0	-	Yes
28	1006.0	599.0	6.2	52.3	55088.8	-	Yes
29	413.0	89.0	10.9	53.8	55100.0	-	Yes
30	970.6	147.8	8.3	130.3	55125.0	-	Yes
31	326.9	1000.1	7.4	54.0	55150.0	-	Yes
32	681.1	908.2	6.3	83.9	55150.0	-	Yes
33	474.3	380.4	9.4	179.5	55160.0	-	Yes
34	25.4	848.4	7.1	18.8	55200.0	-	No
35	442.8	924.7	7.2	85.0	55238.0	-	Yes
36	571.7	833.2	6.7	29.2	55300.0	-	Yes
37	88.3	623.5	6.5	13.6	55374.0	-	No

N	X	Y	Radius	Flux	Appearance (MJD)	Appearance Window (Days)	Flagged
38	9.7	678.3	7.2	16.2	55402.7	-	No
39	59.8	846.3	6.3	15.2	55402.7	-	No
40	145.0	148.0	8.0	<13.1	55402.7	-	No
41	166.0	652.0	8.0	<13.1	55402.7	-	No
42	211.0	842.3	6.1	16.4	55402.7	-	No
43	258.7	655.6	7.0	18.7	55402.7	-	No
44	283.2	1001.3	5.1	14.6	55402.7	-	No
45	284.0	271.0	8.0	<13.1	55402.7	-	No
46	284.4	439.4	6.9	15.3	55402.7	-	No
47	305.0	268.0	8.0	<13.1	55402.7	-	No
48	341.8	785.7	7.2	24.3	55402.7	-	No
49	380.1	461.7	7.4	19.7	55402.7	-	No
50	385.6	488.3	6.0	13.4	55402.7	-	No
51	388.6	734.3	5.6	14.7	55402.7	-	No
52	422.9	913.4	5.8	20.1	55402.7	-	No
53	427.0	79.0	8.0	<13.1	55402.7	-	No
54	435.5	877.1	5.8	19.6	55402.7	-	No
55	453.1	277.2	7.3	17.4	55402.7	-	No
56	495.4	850.6	5.0	15.3	55402.7	-	No
57	503.3	438.1	7.0	19.4	55402.7	-	No
58	525.6	766.8	5.0	14.3	55402.7	-	No
59	557.5	749.3	5.4	17.1	55402.7	-	No
60	561.1	793.2	7.3	32.7	55402.7	-	Yes
61	577.5	884.6	5.1	17.8	55402.7	-	No
62	582.1	807.0	6.5	27.1	55402.7	-	Yes
63	607.3	906.2	5.2	19.7	55402.7	-	No
64	614.7	355.6	6.3	16.2	55402.7	-	No
65	624.6	362.9	6.1	15.3	55402.7	-	No
66	632.0	980.9	5.2	23.1	55402.7	-	No
67	633.8	507.4	6.7	21.4	55402.7	-	No
68	682.9	656.5	5.0	15.2	55402.7	-	No
69	702.8	795.0	5.5	21.8	55402.7	-	No
70	723.5	196.4	6.5	16.3	55402.7	-	No
71	736.0	623.8	5.6	19.4	55402.7	-	No
72	738.3	643.2	5.6	19.9	55402.7	-	No
73	749.3	769.0	4.2	13.1	55402.7	-	No
74	750.3	187.3	6.0	14.0	55402.7	-	No
75	752.6	961.4	3.7	13.3	55402.7	-	No
76	781.0	849.7	4.3	15.7	55402.7	-	No
77	800.9	496.0	6.9	26.9	55402.7	-	Yes
78	803.0	562.7	5.0	15.4	55402.7	-	No
79	805.8	703.8	5.2	19.6	55402.7	-	No
80	813.4	586.8	6.1	23.8	55402.7	-	No
81	814.4	641.3	5.8	22.7	55402.7	-	No
82	821.0	629.2	6.2	26.4	55402.7	-	Yes
83	824.6	584.9	7.0	31.9	55402.7	-	Yes
84	830.2	813.6	3.9	13.7	55402.7	-	No
85	832.0	376.5	5.5	15.5	55402.7	-	No
86	841.3	511.9	5.4	17.8	55402.7	-	No
87	851.6	305.7	6.7	22.0	55402.7	-	No
88	856.3	903.6	4.0	17.0	55402.7	-	No
89	861.1	885.4	4.0	16.1	55402.7	-	No
90	874.9	755.1	5.6	27.6	55402.7	-	Yes
91	880.7	601.8	5.3	20.3	55402.7	-	No
92	886.2	425.4	5.4	16.7	55402.7	-	No
93	891.6	649.0	4.5	15.6	55402.7	-	No
94	897.0	828.2	5.0	25.1	55402.7	-	No
95	898.7	537.2	4.7	14.6	55402.7	-	No
96	904.0	441.5	4.8	14.0	55402.7	-	No
97	908.0	680.6	4.9	19.6	55402.7	-	No
98	915.3	285.7	6.9	24.1	55402.7	-	No
99	926.2	272.9	6.5	21.3	55402.7	-	No
100	958.3	836.7	3.8	16.2	55402.7	-	No
101	965.7	796.9	3.7	16.0	55402.7	-	No
102	979.3	952.6	3.7	18.6	55402.7	-	No
103	1003.7	432.1	5.6	20.8	55402.7	-	No

N	X	Y	Radius	Flux	Appearance (MJD)	Appearance Window (Days)	Flagged
104	1004.8	463.4	4.3	13.1	55402.7	-	No
105	1006.9	862.9	3.7	17.3	55402.7	-	No
106	1009.5	444.5	4.7	14.9	55402.7	-	No
107	264.9	511.1	9.7	78.0	55754.0664	-	Yes
108	329.7	309.3	6.8	14.0	55754.1	-	No
109	1007.0	667.0	5.9	42.4	55796.7	-	Yes
110	512.2	627.8	8.2	57.1	55800.0	-	Yes
111	783.0	339.7	8.2	78.9	55800.0	-	Yes
112	253.0	778.0	8.6	78.8	55806.0	-	Yes
113	15.3	662.7	9.7	29.3	55811.9	-	Yes
114	553.0	70.0	9.2	25.3	55811.9	-	No
115	216.4	170.7	9.0	14.9	55841.3	-	No
116	436.7	293.2	9.9	83.4	55863.0	-	Yes
117	296.1	645.2	9.0	100.3	55898.2969	-	Yes
118	676.9	887.4	5.8	26.9	55898.2969	-	Yes
119	191.5	690.8	6.2	14.4	55898.3	-	No
120	742.7	366.1	5.5	13.9	55996.2	-	No
121	252.2	223.9	7.7	15.6	56082.0	-	No
122	887.4	760.6	4.9	21.5	56082.0	-	No
123	904.6	733.6	4.3	16.1	56246.8	1.4066	No
124	165.8	564.3	9.9	36.1	56327.2852	1.1487	Yes
125	102.9	839.3	9.0	62.7	56370.3633	7.9957	Yes
126	576.0	59.0	7.7	18.1	56464.89	0.0014	No
127	582.1	524.1	6.0	16.6	56464.89	0.0014	No
128	340.0	398.0	7.2	17	56530.1606	0.8553	No
129	87.0	414.0	8.0	n/a	57196.9504	0.3945	No
130	279.0	602.0	7.0	16	57379.4345	0.792	No
131	276.0	583.0	7.0	n/a	57664.1565	0.4704	No
132	495.0	528.0	8.0	n/a	57693.5125	1.0501	No
133	962.0	494.0	6.7	26	57857.4647	3.5168	No
134	969.0	476.0	7.5	95	57939.3281	1.9332	Yes
135	853.0	283.0	8.0	26	57942.252	0.9172	No
136	434.0	770.0	4.9	13	57962.8495	1.7942	No
137	566.0	874.0	6.9	35	57978.4207	1.9643	Yes
138	737.0	952.0	5.2	25	58045.9132	4.6416	No
139	438.0	643.0	6.7	20	58062.4709	4.6187	No
140	853.0	711.0	9.0	180	58062.4709	4.6187	Yes
141	695.0	520.0	8.0	95	58073.536	5.6079	Yes
142	352.0	122.0	10.0	26.3	58106.1018	0.4593	Yes
143	955.0	360.0	6.4	24	58121.2071	12.1979	No
144	268.0	613.0	9.0	30	58174.1477	2.1127	Yes
145	404.0	801.0	6.1	19	58174.1477	2.1127	No
146	736.0	151.0	6.3	15	58188.3145	5.8103	No
147	524.0	906.0	5.6	21	58297.572	2.5189	No
148	519.0	143.0	10.2	130	58309.3771	0.7118	Yes
149	256.0	121.0	10.3	26.3	58464.9916	3.7742	Yes
150	253.0	201.0	11.1	35	58804.1055	8.0801	Yes
151	332.2	711.8	8.6	57	59047.7136	0.3969	Yes
152	173.0	592.6	9.8	159.7	59378.3025	36.3957	Yes
153	997.2	305.0	7.5	95	59860.3405	0.795	Yes

Table 2: All of the WFC3/IR bad pixel tables created to incorporate new blobs. An updated BPIXTAB is only created if a new blob is deemed strong enough (see Section 5). All WFC3/IR observations after a given USEAFTER date use the corresponding BPIXTAB in the *calwf3* pipeline.

BPIXTAB	USEAFTER	USEAFTER (MJD)
35620238i_bpx.fits	Jul 31 2009 00:00:00	55043.000
3562019ii_bpx.fits	Aug 07 2009 00:00:00	55050.000
3562017pi_bpx.fits	Aug 16 2009 00:00:00	55059.000
35620104i_bpx.fits	Aug 30 2009 00:00:00	55073.000
35620295i_bpx.fits	Sep 14 2009 19:12:00	55088.800

3562007mi_bpx.fits	Sep 26 2009 00:00:00	55100.000
35620223i_bpx.fits	Oct 21 2009 00:00:00	55125.000
35620294i_bpx.fits	Nov 15 2009 00:00:00	55150.000
3562029gi_bpx.fits	Nov 25 2009 00:00:00	55160.000
3562006pi_bpx.fits	Feb 11 2010 00:00:00	55238.000
3562020ii_bpx.fits	Apr 14 2010 00:00:00	55300.000
3562030ki_bpx.fits	Jul 25 2010 16:48:00	55402.700
3562029ai_bpx.fits	Jul 12 2011 01:35:36	55754.066
3562028pi_bpx.fits	Aug 23 2011 16:48:00	55796.700
3562007ki_bpx.fits	Aug 27 2011 00:00:00	55800.000
35620322i_bpx.fits	Sep 02 2011 00:00:00	55806.000
3562015ii_bpx.fits	Sep 07 2011 21:36:00	55811.900
35620105i_bpx.fits	Oct 29 2011 00:00:00	55863.000
3562022mi_bpx.fits	Dec 03 2011 07:07:32	55898.297
3562012oi_bpx.fits	Feb 04 2013 06:50:41	56327.285
35620330i_bpx.fits	Mar 19 2013 08:43:09	56370.363
3562032ki_bpx.fits	Jul 05 2017 07:52:27	57939.328
3562022fi_bpx.fits	Aug 13 2017 10:05:48	57978.421
3562028ni_bpx.fits	Nov 05 2017 11:18:05	58062.471
3562018mi_bpx.fits	Nov 16 2017 12:51:50	58073.536
35620297i_bpx.fits	Dec 19 2017 02:26:35	58106.102
3562030bi_bpx.fits	Feb 25 2018 03:32:41	58174.148
3562008pi_bpx.fits	Jul 10 2018 09:03:01	58309.377
3562022ni_bpx.fits	Dec 12 2018 23:47:54	58464.992
3cb1627mi_bpx.fits	Nov 11 2019 02:31:55	58804.106
47m1519ni_bpx.fits	Jul 17 2020 17:07:35	59047.714
57m1910ei_bpx.fits	Jun 13 2021 07:15:36	59378.303
71c1928ri_bpx.fits	Oct 08 2022 08:10:19	59860.341

Revisions

September 4, 2018: We found that some of the oldest blobs (those before the dark-Earth flat monitoring began in July 2010) had inaccurate appearance dates. To correct these dates, we scrolled through early WFC3/IR data to find the image where the blob first appeared and, if this image was taken before the recorded appearance date, we updated the appearance date accordingly. An example of this is the blob at (x, y)=(235.8, 423.1), whose appearance date was listed as July 6, 2010 but is clearly seen in dataset ib5t01ujq which was taken August 7, 2009. Also, three blobs had recorded appearance dates before the exposure time of the first image where blobs could conceivably be seen (i.e. the default MJD=55043). Since we didn't see these blobs before this time, we updated their appearance dates to this default value as was done for many of the other early blobs. The following table summarizes these changes (note: the original appearance dates here correspond to those listed in McCullough et al. (2014)):

X	Y	Radius	Flux	Original Appearance (MJD)	Updated Appearance (MJD)	Flagged
235.8	423.1	10.2	159.7	55383.5	55050.0	Yes
442.8	924.7	7.2	85.0	55250.0	55238.0	Yes
134.1	971.5	8.3	181.4	55187.5	55073.0	Yes
474.3	380.4	9.4	179.5	55175.0	55160.0	Yes
52.0	13.0	12.7	50.0	55071.0	55043.0	Yes
308.0	52.0	10.4	26.4	55038.5	55043.0	Yes
568.0	840.5	4.6	13.7	55042.99	55043.0	No
358.1	762.8	8.2	130.3	55042.99	55043.0	Yes

October 10, 2018: After noticing that the extent of blob #13 wasn't fully masked in deep IR sky flats (Figure 6), we updated its position and radius as summarized below.

Original X	Original Y	Original Radius	Updated X	Updated Y	Updated Radius
569.2	707.0	5.4	571.5	706.5	10.0

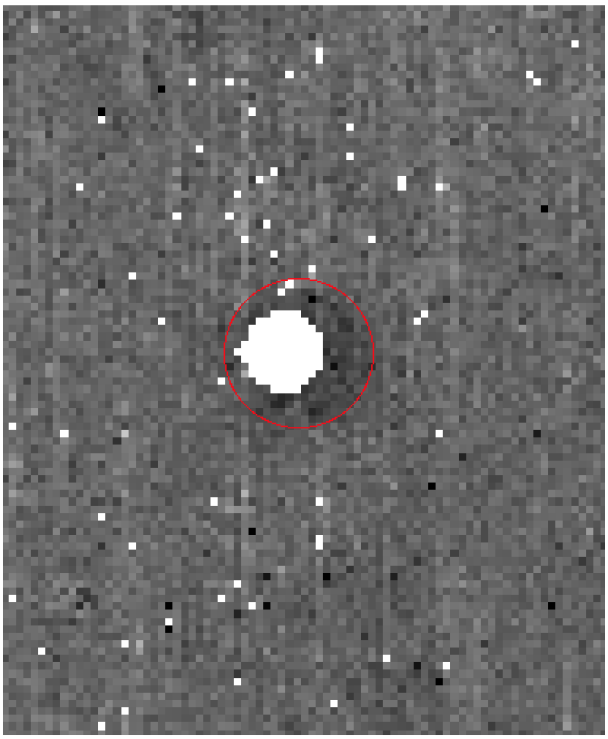

Figure 6: A cutout of a deep F160W IR sky flat where the old mask for blob #13 is shown in white. As seen in the cutout, this old mask misses some of the wings of this blob. We therefore updated this blob's position and radius to better reflect the blob's extent - resulting in the new mask outlined in red.

December 17, 2018: Table 1 was re-sorted to better handle ties, i.e. blobs with the same appearance dates. Now, whenever blobs have the same appearance date, they are sorted by their X value, then Y value. This means that the number (N) of some blobs has changed.

May 8, 2019: Table 2 was updated after the new bad pixel table delivery described in WFC3 ISR 2019-03.

December 11, 2019: A new blob was discovered and a new bad pixel table was delivered. Figures 3, 4, 5, and Tables 1, and 2 were updated accordingly. - Jennifer V. Medina

July 21, 2020: A new blob was discovered and a new bad pixel table was delivered. Figures 3, 4, 5, and Tables 1, and 2 were updated accordingly. - Jennifer V. Medina

August 3, 2021: A new blob was discovered after the HST returned from safe mode and a new bad pixel table was delivered. Figures 3, 4, 5, and Tables 1, and 2 were updated accordingly. - Jennifer V. Medina

October 13, 2022: A new blob was discovered and a new bad pixel table was delivered. Figures 3, 4, 5, and Tables 1, and 2 were updated accordingly. - Benjamin J. Kuhn